JACS
JOURNAL OF THE AMERICAN CHEMICAL SOCIETY

ARTICLE

pubs.acs.org/JACS

In Situ Antibody Detection and Charge Discrimination Using Aqueous Stable Pentacene Transistor Biosensors

Hadayat Ullah Khan,*[,†] Junhyuk Jang,[‡] Jang-Joo Kim,*[,‡] and Wolfgang Knoll[†,§]

[†]Material Science Group, Max-Planck Institute for Polymer Research, Ackermannweg-10, D-55128 Mainz, Germany
[‡]OLED Center, Department of Materials Science and Engineering, Seoul National University, Seoul 151-744, Korea
[§]AIT Austrian Institute of Technology GmbH, Donau-City-Strasse 1, 1220 Vienna, Austria

Supporting Information

ABSTRACT: Pentacene-based organic thin-film transistors were used to create highly sensitive, real-time electronic sensors for selective antibody detection. Bovine serum albumin was covalently attached to a modified pentacene surface to selectively detect the label free monoclonal antiBSA. These sensors displayed a high affinity constant (K_A) of $(1.1 \pm 3) \times 10^7$ M^{-1} at pH 7, which is 1 order of magnitude higher than those obtained with a highly sensitive surface plasmon resonance spectroscopy detection system. Furthermore, a high degree of discrimination in the hybrid antiBSA charges was achieved at different pH values. This demonstration of fast, label-free, real-time detection of nanoscale biomolecules in aqueous buffer solutions using the organic transistor sensing platform will have a significant impact on high-performance microarrays in addition to discriminating the presence of ionizable groups.

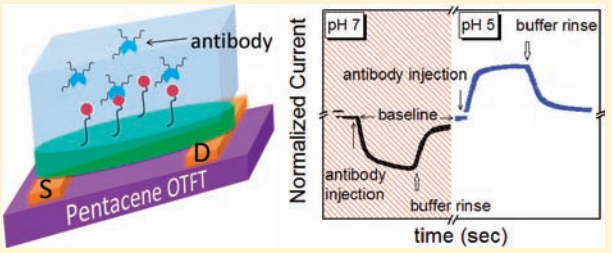

INTRODUCTION

Over the last 5 decades, it has been widely recognized that an antibody populations need to be defined not only in terms of its quantity, but also in terms of its affinity, or the strength with which it binds to the corresponding antigenic determinant.[1] Both factors are important for the wide application of gene therapy,[2] single-molecule enzymology, microarrays, microchips,[3] and pH effect.[4,5] Unfortunately, quantitative determination of antigen/antibody binding parameters traditionally has been a laborious endeavor. Even though a recent development in surface plasmon resonance (SPR) technology has greatly simplified this task,[6] it is time-consuming and expensive, making the technique difficult for point-of-need and high-throughput applications.[7,8] Hence, there is a need to develop label-free, rapid, highly selective and sensitive detection platforms.

Organic thin-film transistors (OTFTs) have gained considerable attention with the demonstration of potentially scalable patterning process.[9] Although the performance of OTFTs have improved remarkably over the past 2 decades, the degradation of electrical performance in ambient air/buffer solution is a significant problem in need of a solution for implementation in commercial devices. Passivation of OTFTs has become a common and widely investigated approach using single or multilayers of organic/polymer materials.[10] Recent advances in chemical detection research, in part benefitting from the overwhelming progress made in nanotechnology and organic electronics, have shown great promise for a viable, low-cost alternative to current optical detection systems.[11] Many examples exist for the detection of analyte vapors using an OTFT platform, with numerous reports addressing the ability to identify particular analytes either through the use of a fingerprint response[12,13] or by incorporating selective detection layers on functional OTFTs;[14] however, these devices were not selective toward a particular analyte. Selective in situ detection with OTFTs requires a versatile method for the immobilization of various selective molecular probes, which is not a trivial task. Additionally, it is well-known that most microorganisms possess a negative surface charge under physiological conditions.[15] Therefore, developing complementary tools for probing analyte surface charges on a nanoscale level is a highly relevant challenge in cellular microbiology and biophysics.

This paper reports on a real-time and selective immunodetection platform based on a modified pentacene transistor. The surface of the pentacene was modified with plasma-enhanced chemical vapor deposition (PE-CVD) of perfluor-1,3-dimethylcyclohexan (PFDMCH) and maleic anhydride (MA) layers to passivate and chemically functionalize the OTFT surface, respectively. Bovine serum albumin (BSA) was covalently attached to the ppMA functional layer as a catcher probe and proven to be effective for the detection of antibodies.[3] AntiBSA was selectively detected using OTFTs, and the results were corroborated with a well-characterized optical detection method, SPR. We also show that the isoelectric point (pI) of the proteins can be estimated using the transistor sensor because it provides a method of discriminating between the charges of the analytes in a 10 mM concentrated buffer solution of different pH's.

Received: August 7, 2010
Published: January 31, 2011

ACS Publications © 2011 American Chemical Society

dx.doi.org/10.1021/ja107088m | J. Am. Chem. Soc. 2011, 133, 2170–2176

Scheme 1. Schematic Representation of a Bottom-Contact Pentacene OTFT and Optical Sensors[a]

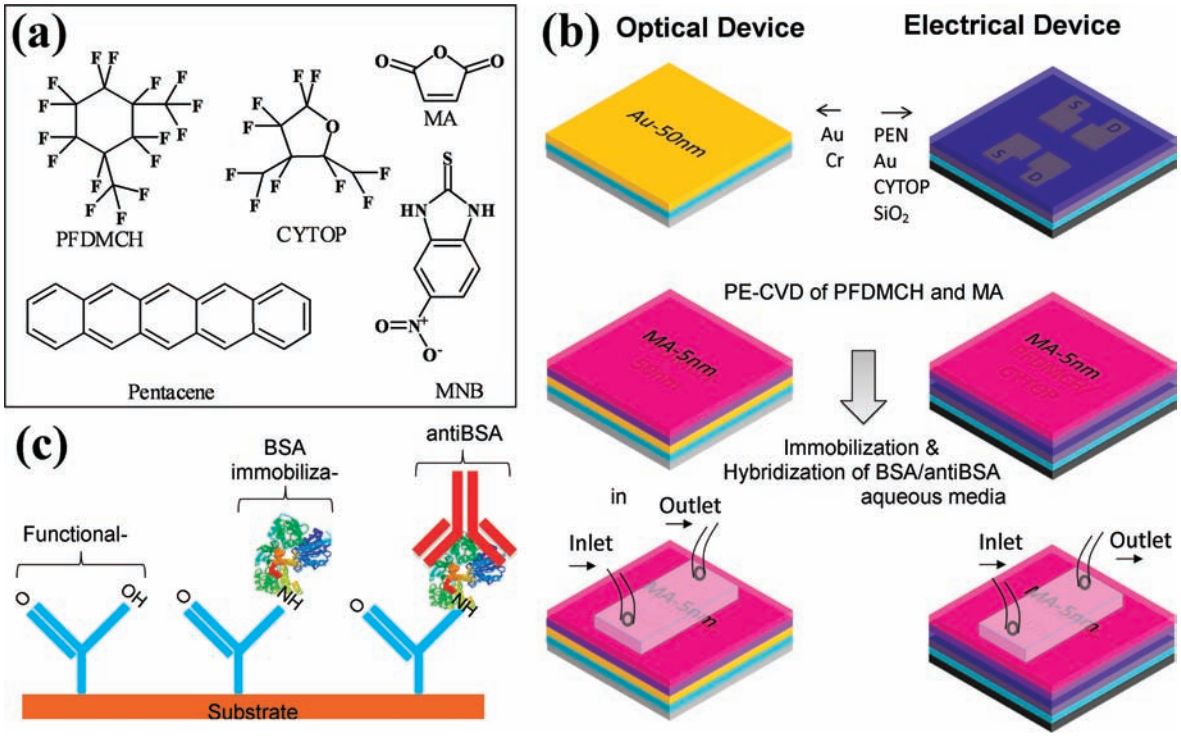

[a] (a) Chemical structure of the organic molecules. (b) (Right, top to bottom) Fabrication procedure for a bottom-contact OTFT with CYTOP (15 nm)/SiO_2 (200 nm) dielectric layer, source-drain electrodes with a W/L of 10 and a 30 nm pentacene layer followed by the top PE-CVD protective and functional layer. (Left, top to bottom) Fabrication procedure for the optical device with Au (50 nm)/Cr (2 nm)/LaSFN9 glass followed by the top identical PE-CVD protective and functional layer. (c) Schematics of the surface modification to immobilize the BSA for selective antiBSA detection.

MATERIALS AND METHODS

Materials. All materials were purchased from Sigma Aldrich and used as received unless stated otherwise. *N*-Ethyl-*N*′-(3-(dimethylamino)propyl)carbodiimide hydrochloride (EDC) and *N*-hydroxysuccinimide (NHS) were purchased from Fluka. Bovine serum albumin (BSA) (MW ~66 kDa) and rabbit monoclonal antiBSA were obtained from Millipore. Sodium acetate buffer solutions (ABS) (10 mM concentrated at pH 7 and pH 5) were freshly prepared for use with the biosensing experiments.

Electrical and Optical Device Fabrication. A heavily doped silicon wafer was used to fabricate the bottom-contact OTFTs (see Scheme 1b, device structure and fabrication schemes). The substrates were cleaned using acetone, 2-propanol, ethanol; rinsed with deionized water; and then baked at 100 °C for 5 min. CYTOP solution (1 wt %) was spin-coated at 4000 rpm for 40 s in an Ar-filled glovebox and baked at 80 °C for 30 min and 180 °C for 1 h to achieve a required thickness of 15 nm. CYTOP insulating films have already proven to be highly stable in air and moisture,[16] with a surface roughness of 0.6 nm, as determined by AFM (NanoScope Dimension 3100 CL) (Supporting Information, Figure S2a). Fifty nanometer thick source-drain electrodes with a width (W) of 500 μm and length (L) of 50 μm were deposited and patterned using a shadow mask. The Au electrodes were treated for 1 h with 0.1 mM solution of 2-mercapto-5-nitrobenzimidazole (MNB) diluted in ethanol to reduce the contact resistance.[17] Finally, a 30 nm thick pentacene film was thermally deposited under a pressure of 6.5×10^{-7} mbar with a deposition rate of 0.5 Å/s at a surface temperature of 30 °C and displays a surface peak-to-valley roughness of 30 nm (Supporting Information, Figure S2b,c). The optical device fabrication (Scheme 1b), identical to that of the OTFTs, was done using similar procedures as previously reported.[18]

PE-CVD Reactor and Thin-Film Characterization. The polymerization of PFDMCH and MA was carried out in a home-built PE-CVD reactor.[18] Additional details on the reactor can be found in the Supporting Information (Figure S1).

Flow Cell. Sensor measurements were done in a flow cell made of Plexiglas (Figure 1a)[18] and are provided in the Supporting Information.

Electrical and Optical Characterizations. All electrical measurements were performed with a Keithley 4200 semiconductor characterization system in ambient air and aqueous media. The optical detection was done with a home-built surface plasmon resonance (SPR) spectroscopy.[19]

RESULT AND DISCUSSION

Pentacene has become the most widely studied organic semiconductor due to its excellent transport properties; however, it suffers from poor stability in ambient conditions.[20] Air-stable bottom contact OTFTs with a 30 nm thick pentacene layer on an ultrathin CYTOP (15 nm) layer[21] were fabricated and then spin-coated on the Si substrate covered with 200 nm thick SiO_2 (Scheme 1b). The device exhibited excellent linear and saturation regime characteristics with a V_{DS} of −50 V, an average mobility of 0.116 cm^2/V s, an on/off ratio of 10^6, and a threshold voltage (V_{th}) of −4.8 V. The transfer and output characteristics of these devices are displayed in Figure 1b.

Electrical and sensing measurements in the buffer solutions were done using a flow cell (Figure 1a), which was laminated on the PE-CVD-treated OTFT surface. Organic semiconductors in general are sensitive to aqueous buffer solutions; therefore, it is a

challenging task to passivate or functionalize their surface without degrading their electrical performance. To eliminate potential degradation arising from solution chemistry, PE-CVD was used to prepare a perfluorinated polymer film (50 nm, ppPFDMCH) for surface passivation and a 5 nm thick maleic anhydride (ppMA) functional layer to covalently attach the BSA. The structural formulas of the materials are given in Scheme 1a and Figure S3 (Supporting Information). PE-CVD provides a single-step process at room temperature, resulting in a conformal coating with excellent adhesion to the underlying film.[18] Additional details on the PECVD films, including Fourier transform infrared spectroscopy (FTIR) (Figure S4) and X-ray photoelectron spectroscopy (XPS) (Figure S5) results are described in the Supporting Information. The thickness of the encapsulation layer was optimized within the range of 30−50 nm to obtain stable characteristics in buffer solutions (Supporting Information, Figure S6).

In the presence of a buffer solution (pH 7, 10 mM), the anhydride groups on the ppMA surface were hydrolyzed and converted to carboxylic acids and then activated by circulating a solution containing 0.2 M EDC and 0.05 M NHS at a constant rate of 300 μL/min for 20 min. BSA was covalently attached to the surface from a 1 μM BSA solution for 80 min, after which any nonchemically bound material was rinsed with buffer solution. The transfer characteristics in air at a V_{DS} of −5 V showed a shift in V_{th} after the PE-CVD treatment (Supporting Information, Figure S8), which can be attributed to charge trapping at the interface during the deposition process.[22] Moreover, the OTFT drain current decreased after BSA attachment due to the negative charges on the BSA proteins under the given operating conditions (Supporting Information, Figure S8).[23] Control experiments were carried out to confirm the covalent attachment of BSA with the sensors surface using in situ SPR measurements (see Supporting Information, Figure S9). The specificity of these sensors toward the antibody was evaluated using antiBSA. The binding protocol for this process is shown in Scheme 1c.

Prior to sensor analysis, the functional OTFT surface was characterized in ambient and buffer conditions. We observed an increase in the source-drain current (I_{DS}) in buffer solution (black dashed curve) compared to ambient air (black solid curve, Figure 1c) at a low drain voltage of −5 V, which is necessary for operation in the buffer solution. The output plots are shown in the Supporting Information (Figure S7). The slight variation in the transfer characteristics illustrates a relatively stable behavior with a small change in mobility from 0.006 cm^2/V s in ambient air to 0.0052 cm^2/V s in the buffer solution. This indicates that the passivation by the thin perfluorinated polymer layer is very effective to protect the pentacene layer from water permeation.[21,24] The increase in the drain current under solution can be attributed to the effect of water on the sensor.[18] Even though the current flow through the buffer solution cannot be totally excluded for the increase of the drain current, the current does not influence the sensing as demonstrated below.

Antigen/antibody interactions belong to a large group of noncovalent biological binding reactions, which depend mainly on complementary structures between a ligand and a binding site (receptor) on a macromolecule. Since the antigen and antibody consist of amino acids bearing charges, we expect that the polarity of these charges strongly depends on the pH and ionic strength of the aqueous phase, which determines the charged states and binding kinetics. This polarity is normally defined by the isoelectric point (pI) of a respective analyte. The pI of the bovine

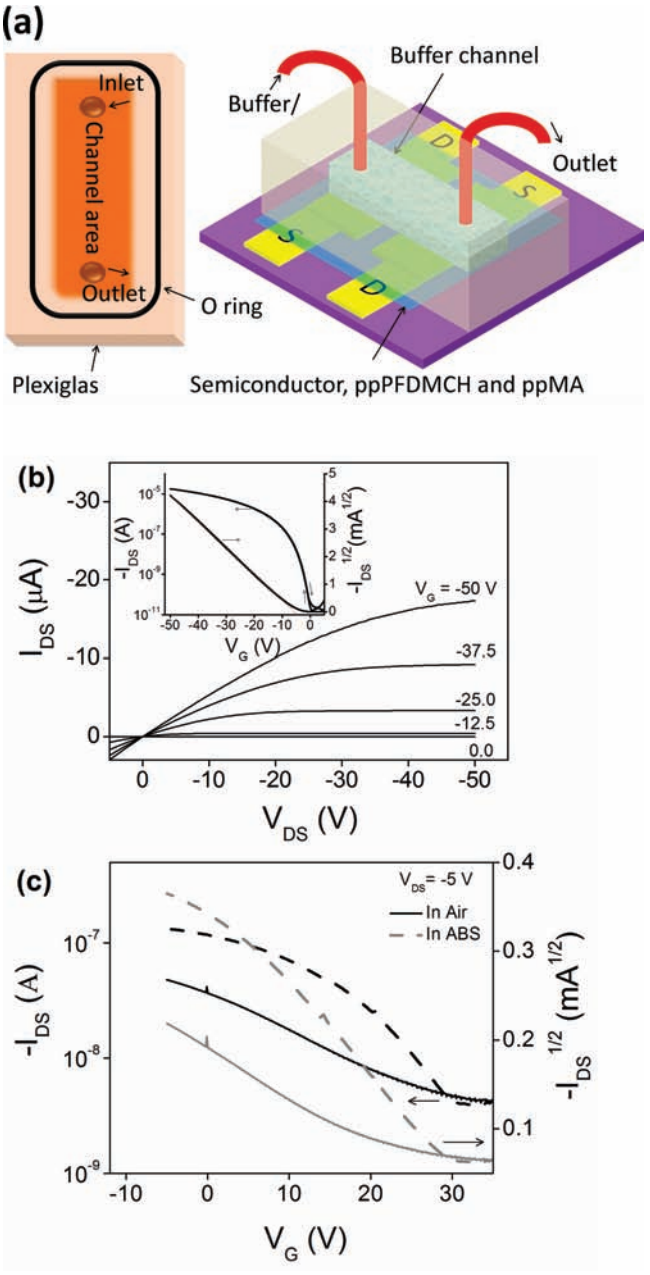

Figure 1. (a) Schematic of an OTFT and a flow cell configuration for protein sensing in an aqueous buffer medium. (b) Output characteristics (I_{DS} vs V_{DS}) with various V_G. (Inset) Transfer characteristics (I_{DS} vs V_G) at a constant V_{DS} of −50 V in ambient conditions of a representative bottom-contact OTFT with 30 nm pentacene on 15 nm CYTOP/200 nm SiO_2 with an electrode geometry (W/L) of 10. (c) Transfer characteristics (I_{DS} vs V_G) of the same device at constant V_{DS} of −5 V under ambient conditions (solid curve) and immediately after injection of the buffer solution (dashed curve). See Supporting Information (Figure S7) for corresponding output plots.

serum is at pH 5.4, which means that the amino acids within the BSA proteins will contain (on average) negative charges above this pH.[25] We expect that negatively charged BSA proteins will result in a decrease in the current during sensor operation and vice versa.

The sensor performance of the OTFTs was evaluated under constant bias conditions. The change in current was recorded

dx.doi.org/10.1021/ja107088m |J. Am. Chem. Soc. 2011, 133, 2170–2176

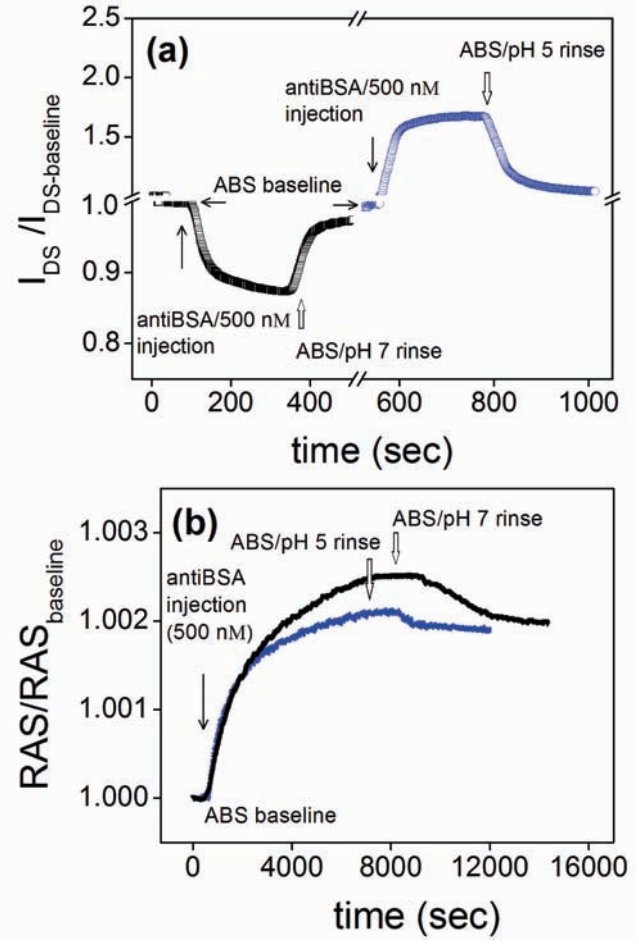

Figure 2. Charge discrimination experiments for BSA/antiBSA immunoassay formation in aqueous buffer solutions at different pHs using OTFT and SPR sensors. The solid arrows indicate an injection of antiBSA and open arrows indicate exchange with pure buffer solution. (a) OTFT current response ($I_{DS}/I_{DS\text{-baseline}}$) with time upon exposure to antiBSA (500 nM) diluted in buffer solution at pH 7 (black curve) and at pH 5 (blue curve) while operating at a constant bias ($V_G = -5$ V, $V_{DS} = -2$ V). (b) $RAS/RAS_{baseline}$ response with time upon exposure to antiBSA (500 nM) diluted in buffer solution at pH 7 (black curve) and at pH 5 (blue curve) using SPR sensing platform.

while switching from a baseline buffer solution to one containing a given concentration of antiBSA. Typically, the baseline current was recorded for 100 s with a constant source-drain and gate biases ($V_{DS} = -2$ V, $V_G = -5$ V) prior to analyte injection. A flow rate of 300 μL/min was used to minimize the mass transfer limitations of the analyte to the sensor surface, which has been shown to occur below 20−30 μL/min.[25] The effect of the net charges on the transistor sensor surface is shown in Figure 2a. A 500 nM solution of antiBSA at pH 7 was injected into the flow cell while recording the I_{DS} under constant bias conditions as described above. Equilibrium between the bulk concentration and the corresponding surface coverage was achieved within 250 s, as determined by the source-drain current with the time profile (i.e., I_{DS} is constant after surface equilibrium is achieved). The solution was then switched to the buffer solution (pH 7), and the I_{DS} recovered to the initial baseline current after 130 s (black curve in Figure 2a). Next, a new baseline was established in a 10 mM buffer solution at pH 5. In a similar manner to the pH 7 case, a 500 nM concentrated antiBSA solution diluted in buffer at pH 5 was introduced to the sensor surface while recording the I_{DS} (blue curve in Figure 2a). However, at this pH, the I_{DS} increased as the antiBSA reached the sensor surface, and the sequential exchange of antiBSA with buffer solution (pH 5) resulted in a decrease in the I_{DS}. Two effects on the I_{DS} were observed in response to antiBSA: (a) the magnitude of the change in current (ΔI_{DS}) at pH 7 was a factor of 5 time less than at pH 5, and (b) the polarity of the current change was opposite at pH 7 from pH 5. These experimental results are consistent with our initial hypotheses that an opposite change in current would occur above and below the p*I*.

For comparison purposes, optical measurements were taken using a home-built SPR spectroscopy[19] to corroborate the OTFT response on an identical substrate (Scheme 1b). SPR spectroscopy also measures the label-free binding by directly monitoring the change in the refractive index at the biosensor surface, and the response is proportional to the mass of the bound analytes.[6] In a typical optical measurement, a kinetic scan of the minimum resonance angle shift (RAS) with time is performed. The black curve in the Figure 2b shows the change in RAS after injection of 500 nM antiBSA and during the formation of the immunoassay, which occurred over a period of 150 min. Careful rinsing with buffer solution (pH 7) was then performed, showing a small effect on the adsorbed antiBSA layer thickness. A similar experiment was done using antiBSA diluted in pH 5 buffer solution with the same concentration (blue curve). Clearly, the SPR measurements could not discriminate between the polarities of the charged states in the antiBSA.

Apart from charge discrimination, the surface titration experiments were also performed to quantify the amount of antiBSA selectively adsorbed on the sensor surface. The change in I_{DS} with time contains kinetic information on the immunoassay and can be analyzed to determine association (k_{on}) and dissociation (k_{off}) rate constants. The general procedure begins with injecting an analyte solution at low concentration and allowing the adsorption of antiBSA onto BSA to reach equilibrium. This process is repeated with higher concentrations until the surface is saturated with the target analyte. In the first experiment, a baseline current was established in 10 mM buffer solution (pH 7) followed by a solution exchange with a 10 nM solution of antiBSA at pH 7. I_{DS} was measured until equilibrium was achieved, as indicated by the constant source-drain current. Next, solutions with concentrations of 50, 100, 200, 500, and 1000 nM antiBSA were injected into the flow system (see thin arrows in Figure 3a), which resulted in correspondingly higher equilibrium surface coverage. Finally, the antiBSA solution was exchanged by the buffer solution (pH 7) in order to dissociate the bound species. Similar surface titration measurements were repeated with antiBSA in buffer solutions at pH 5. As shown in Figure 3b, surface coverage equilibrium was achieved at a rather high concentration of antiBSA at pH 5. In each case (Figure 3a,b), a rapid decrease in the I_{DS} was observed within the initial 40 s after the antiBSA solution was replaced by the buffer solutions, owing to the removal of physisorbed antiBSA, which accounted for 35% and 51% of the equilibrated I_{DS} at pH 7 and pH 5, respectively.

In order to validate the performance of the electronic device, kinetic titration measurements were taken using SPR, where the RAS was measured for various antiBSA concentrations at pH 7 and pH 5 (Figure 3c,d). The reflectivity vs incident angle measurement before and after the BSA/antiBSA immunodetection were fit using Fresnel simulation software (Winspall 2.0) to

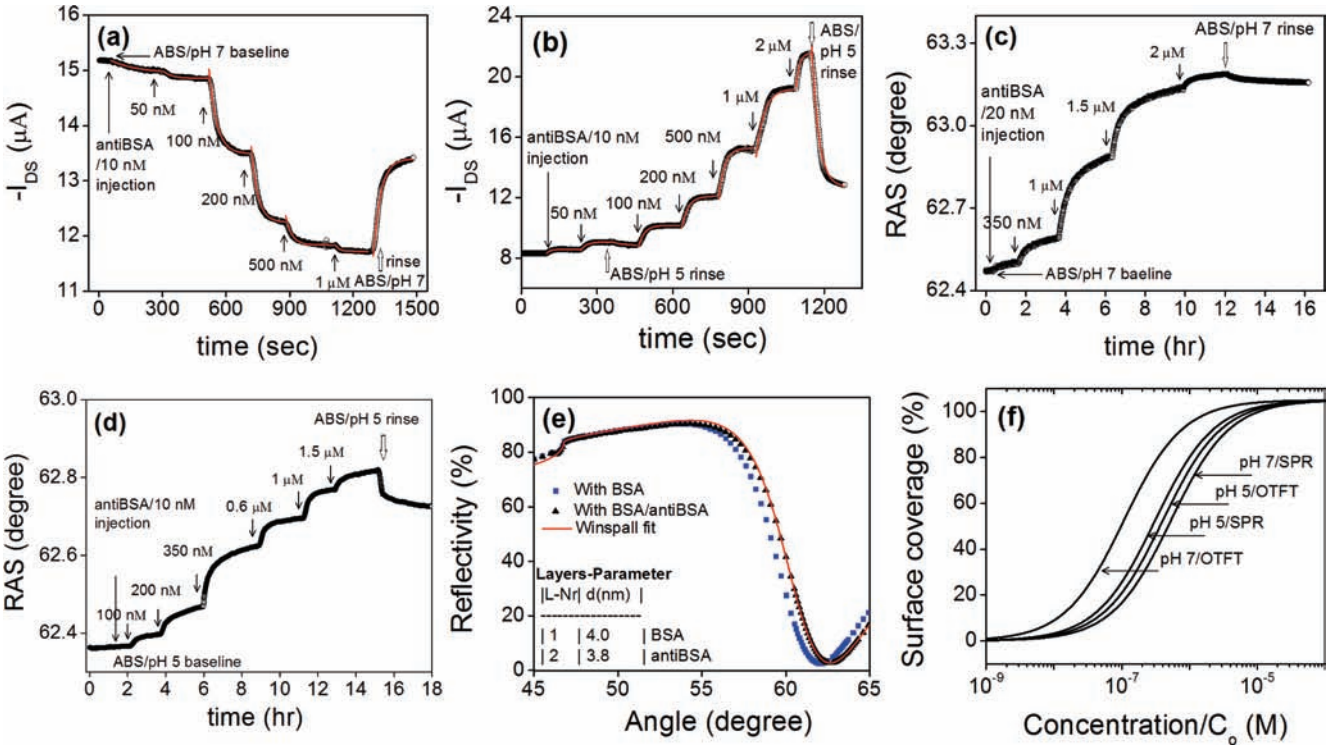

Figure 3. Titration curves for BSA/antiBSA immunoassay formation using OTFT and optical sensors. Solid arrows indicate the additions of antiBSA solutions and open arrows indicate the exchange with buffer solution. Red solid curves represent the Langmuir fits. OTFT current response with time upon exposure to antiBSA solutions at (a) pH 7 and (b) pH 5. SPR sensor titration with antiBSA solutions at (c) pH 7 and (d) pH 5. (e) Angular reflectivity measured before (blue dotted curve) and after (black dotted curve) antiBSA immunoassay formation. The red solid curve shows the Winspall fit based on the Fresnel analysis to estimate the optical thickness of the multilayer film. (f) The Langmuir isotherm plot between the surface coverage and antiBSA (analyte) concentration for the data points taken from parts a−d.

determine the change in optical thickness (red solid line shown in Figure 3e). The calculated thicknesses of BSA and antiBSA layers on the OTFT surface were 4 and 3.8 nm, respectively.[26,27] AntiBSA/BSA binding occurred at a much slower rate during the SPR measurements, leading to a time constant of tens of minutes. OTFT sensor measurements showed a 1 order of magnitude faster response time compared to the SPR method, which can be attributed to the enhanced diffusion/adsorption induced by the electric field present during OTFT operation.

During the SPR measurements, only a very small change in RAS was observed upon dissociation of antiBSA (Figures 2b and 3c,d). It is likely that multisite complexes are formed, leading to stronger protein−protein binding through the multiple available sites, mass transport, crowding, or denaturing of protein.[28] These factors introduce additional complexity to the analysis of the protein rate constant that is not directly related to the association or dissociation reactions. Additionally, the events occur on a time scale that cannot accurately be resolved by SPR measurements.[28,29] The accuracy of quantifying the kinetic parameters is limited by the stronger binding observed in the SPR measurements. These limitations do not apply to OTFT sensors, since it is a fast measuring system. Nevertheless, the Langmuir isotherm model was used to extract the kinetic data from the optical titration experiments that relate the surface coverage $\Theta(C_o)$ to concentration (C_o) shown in Figure 3f. The calculated results for k_{on}, k_{off}, and the affinity constant, K_A ($K_A = k_{on}/k_{off}$), based on the Langmuir model[30] are summarized in Table 1. The K_A values obtained using the OTFT sensor were an order of magnitude higher than the SPR sensors and 4 times higher than previously reported values.[3,31] However, Ishikawa et al. showed values 1 order of magnitude higher for the K_A for N-protein using In_2O_3 nanowire transistor based sensors.[32] Regardless, many advantages exist for using organic devices with low-cost and simple processing methods.

Table 1. Rate Constants Determined for OTFT from Figure 3a,b,f and SPR from Figure 3f

antiBSA diluted in variable pH	k_{off} (s^{-1})	k_{on} (M^{-1} s^{-1})	K_A (M^{-1})
OTFT Sensor (Titration and Isotherm Fit)			
pH 7	1.5×10^{-2}	1.6×10^{5}	$(1.1 \pm 3) \times 10^{7}$
pH 5	3.0×10^{-2}	9.0×10^{4}	$(3.0 \pm 2) \times 10^{6}$
Optical/SPR Sensor (Isotherm Fit)			
pH 7			$(1.9 \pm 2) \times 10^{6}$
pH 5			$(4.3 \pm 2) \times 10^{6}$

The effect of pH on the affinity constant is also significant for OTFT sensors. The discrimination factor in K_A found at pH 7 was an order of magnitude higher than at pH 5. Detection with SPR, however, showed a relatively minor difference (less than a factor of 2) between pH 7 and pH 5. During sensor measurements with the OTFTs, the solution pH influences the polarity and magnitude of the drain current response, which is related to protein binding. To explain the differences in the surface charge density of a protein, we propose models for BSA/antiBSA binding in pH 5 (Figure 4a) and in pH 7 (Figure 4b) buffer

dx.doi.org/10.1021/ja107088m |J. Am. Chem. Soc. 2011, 133, 2170–2176

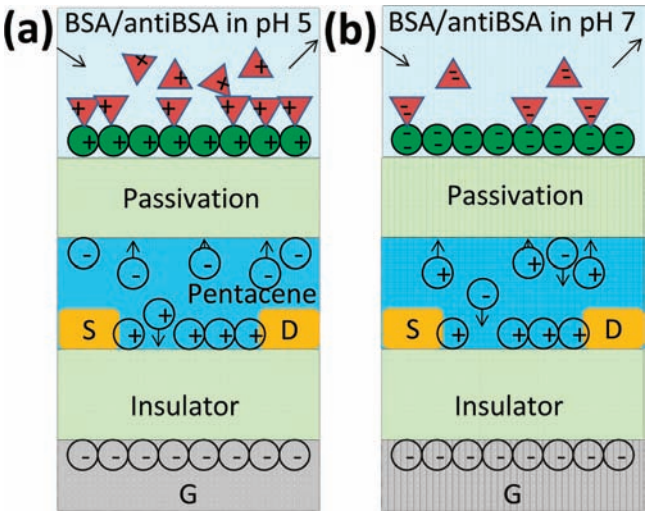

Figure 4. The model for immunodetection using pentacene transistor sensors when antiBSA is diluted in buffer solution at (a) pH 5 and (b) pH 7.

solutions. It has been previously reported that in the case of bovine serum, a change in the electric flux is very small when varying pH below the p*I*.[33] We, therefore, assumed that due to the flux effect, the ratio of NH_2 to NH_3^+ is high below the p*I*, resulting in a weak Coulombic repulsion between BSA and antiBSA. Thus, more antiBSA can adsorb, leading to surface saturation occurring at higher concentrations. This assumption agrees well with the observed experimental data for titration (Figure 3b). The presence of such weak repulsive interactions that are proportional to the square of the surface charges[34] leads to creation of a strong repulsive barrier between transistor channel and the surface-bound analytes (Figure 4a). Ultimately, the holes in the channel region accumulate more efficiently, and an increase in I_{DS} with a larger magnitude of current change (more species adsorbed to influence the current) [Figures 2a (blue curve) and 3b] is seen.

A larger change in electric flux occurs at pH values above the p*I*, which results in a high density of COO^- in the BSA/antiBSA complex and a strong Coulombic repulsion between BSA and antiBSA. This strong electrostatic repulsion allows for a lower density of negative charges at the sensor surface. These low densities of negative charges subsequently show a weak electrostatic interaction between the channel region and the surface negative charges, as shown in Figure 4b. Essentially, the holes are depleted from the channel region of the transistor, increasing the overall channel resistance. Accordingly, we observed a decrease in I_{DS}, but the overall response was comparatively small.

CONCLUSION

We have demonstrated a highly sensitive, low cost, fast, and selective immune−transistor sensor with analyte charge discrimination at variable pH's. A Langmuir model was used to fit the titration curves, which showed that a high affinity constant [$K_A = (1.1 \pm 3) \times 10^7\ M^{-1}$] can be achieved in an organic transistor based detection system when antiBSA was diluted at pH 7. Remarkably, the affinity constant determined at pH 7 was 1 order of the magnitude higher than those obtained on identical substrates using a well-defined optical technique, surface plasmon resonance (SPR) spectroscopy, with the additional advantage of charge discrimination. Due to the fast binding process on the OTFTs sensor surface, one could easily prevent the undesirable reactions that occur during SPR measurements. Our approach appears to have potential for extension into a fully integrated system, providing an inexpensive, fast, and selective sensor platform for a wide range of applications in biomedical use, gene therapy, and microarrays as well as screening for the affinity constant of specific antibodies generated by a library of cells.

ASSOCIATED CONTENT

Supporting Information. PE-CVD based thin-film deposition and its characterization was examined by FTIR and XPS, by in situ immobilization of BSA on an optical SPR sensor surface, and by OTFTs transfer characteristics in ambient air before and after PE-CVD treatment; BSA immobilization and encapsulation's thickness effect on electrical measurements in solution are given in the supporting text and figures. This material is available free of charge via the Internet at http://pubs.acs.org.

AUTHOR INFORMATION

Corresponding Author
khanh@mpip-mainz.mpg.de; jjkim@snu.ac.kr

ACKNOWLEDGMENT

H.U.K. acknowledges the financial support from IRTG/1404 (funded by the DFG) and Max Planck Society, Germany. J.J.K. acknowledges the WCU (R31-2008-000-10075-0) and BSR (R15-2008-006-01001-0) through the NRF funded by the Ministry of Education, Science and Technology Korea. We are also grateful to D. Mossner, IMTEK, University of Freiburg, Germany, for performing the XPS measurements.

REFERENCES

(1) Steward, M. W. *Immunol. Today* **1981**, *2*, 134.
(2) Agrawal, S.; Lyer, R. P. *Curr. Opin. Biotechnol.* **1995**, *6*, 431.
(3) Chiem, N. H.; Harrison, D. J. *Electrophoresis* **1998**, *19*, 3040.
(4) Xavier, K. A.; Willson, R. C. *Biophys. J.* **1998**, *74*, 2036.
(5) Wong, L. S.; Khan., F.; Micklefield, J. *Chem. Rev.* **2009**, *109*, 4025.
(6) Stenberg, E.; Persson, B; Roos, H.; Urbaniczky, C. *J. Colloid Interface Sci.* **1991**, *143*, 513.
(7) Tu, I. P.; Schaner, M.; Diehn, M.; Sikic, B. I.; Brown, P. O.; Botstein, D.; Fero, M. J. *BMC Genomics* **2004**, *5*, 64.
(8) Kingsmore, S. F. *Nat. Rev. Drug. Discovery* **2006**, *5*, 310.
(9) Briseno, A. L.; Mannsfeld, S. C. B.; Ling, M. M.; Liu, S.; Tseng, R. J.; Reese, C.; Roberts, M. E.; Yang, Y.; Wudl, F.; Bao, Z. *Nature* **2006**, *444*, 913.
(10) Han, S. H.; Kim, J. H.; Son, Y. R.; Lee, K. J.; Kim, W. S.; Cho, G. S.; Jang, J.; Lee, S. H.; Choo, D. J. *Electrochem. Solid State Lett.* **2007**, *10*, j68.
(11) Roberts, M. E.; Mannsfeld, S. C. B.; Queralto, N.; Locklin, J.; Knoll, W.; Bao, Z. *Proc. Natl. Acad. Sci. U.S.A.* **2008**, *105*, 12134.
(12) Crone, B.; Dodabalapur, A.; Gelperin, A.; Torsi, L.; Katz, H. E.; Lovinger, A. J.; Bao, Z. *Appl. Phys. Lett.* **2001**, *78*, 2229.
(13) Chang, J. B.; Liu, V.; Subramanian, V.; Sivula, K.; Luscombe, C.; Murphy, A.; Liu, J.; Frechet, J. M. J. *J. Appl. Phys.* **2006**, *100*, 014506.
(14) Torsi, L.; Farinola, G. M.; Marinelli, F.; Tanese, M. C.; Omar, O. H.; Valli., L.; Babudri., F.; Palmisano, F.; Zambonin, P. G.; Naso, F. *Nat. Mater.* **2008**, *7*, 412.
(15) Mozes, N.; Marchal, F.; Hermesse, M. P.; Van Haecht, J. L.; Reuliaux, L.; Leonard, A. J.; Rouxhet, P. G. *Biotechnol. Bioeng.* **1987** *30*, 439.

(16) Walser, M. P.; Kalb, W. L.; Mathis, T.; Brenner, T. J.; Batlogg, B. *Appl. Phys. Lett.* **2009**, *94*, 053303.
(17) Park, D. S.; Jang, W. C.; Cho, S. W.; Seo, J. H.; Jeong, I. S.; Kim, T. W.; Chang, G. S.; Moewes, A.; Chae, K. H.; Jeong, K.; Yoo, K.-H.; Whang, C. N. *Org. Electron.* **2008**, *9*, 1010.
(18) Khan, H. U.; Roberts, M. E.; Johnson, O.; Förch, R.; Knoll, W.; Bao, Z. *Adv. Mater.* **2010**, *22*, 4452.
(19) Knoll, W. *Annu. Rev. Phys. Chem.* **1998**, *49*, 569.
(20) Klauk, H.; Halik, M.; Zschieschang, U.; Schmid, G.; Radlik, W.; Weber, W. *J. Appl. Phys.* **2002**, *92*, 5259.
(21) Jang, J.; Kim, J. W.; Park, N.; Kim, J.-J. *Org. Electron.* **2008**, *9*, 481.
(22) Kang, S.; Park, J.; Jung, S.; Lee, H.-J.; Son, P.; Kim, J. C.; Yoon, T. H.; Yi, M. *Jpn. J. Appl. Phys.* **2007**, *46*, 2696.
(23) Carvalho, L. A.; Carmona-Ribeiro, A. M. *Langmuir* **1998**, *14*, 6077.
(24) Cheng, X.; Caironi, M.; Noh, Y.-Y.; Wang, J.; Newman, C.; Yan, H.; Facchetti, A.; Sirringhaus, H. *Chem. Mater.* **2010**, *22*, 1559.
(25) Adamczyk, M.; Moore, J. A.; Yu, Z. *Methods* **2000**, *20*, 319.
(26) Terashima, H.; Tsuji, T. *Colloids Surf. B. Biointerfaces* **2002**, *27*, 115.
(27) Tronin, A.; Dubrovsky, T.; Nicolini, C. *Thin Solid Films* **1996**, *284*−*285*, 894.
(28) Schreiber, G.; Haran, G.; Zhou, H.-X. *Chem. Rev.* **2009**, *109*, 839.
(29) Rich, R. L.; Cannon, M. J.; Jenkins, J.; Pandian, P.; Sundaram, S.; Magyar, R.; Brockman, J.; Lambert, J.; Myszka, D. G. *Anal. Biochem.* **2008**, *373*, 112.
(30) Langmuir, I. *J. Am. Chem. Soc.* **1918**, *40*, 1361.
(31) Li, B.; Chen, J.; Long, M. *Anal. Biochem.* **2008**, *377*, 195.
(32) Ishikawa, F. N.; Chang, H.-K.; Curreli, M.; Liao, H.-I.; Olson, A. C.; Chen, P.-C.; Zhang, R.; Roberts, R. W.; Sun, R.; Cote, R. J.; Thompson, M. E.; Zhou, C. *ACS Nano* **2009**, *3*, 1219.
(33) Chun, K. Y.; Stroeve, P. *Langmuir* **2002**, *18*, 4653.
(34) Burns, D. B.; Zydney, A. L. *Biotechnol. Bioeng.* **2000**, *64*, 27.